Title

Toward miniaturized analysis of chemical identity and purity of radiopharmaceuticals via microchip electrophoresis

Journal

Analytical and Bioanalytical Chemistry, 410(9)

ISSN

1618-2642

Authors

Ly, Jimmy
Ha, Noel S
Cheung, Shilin
et al.

Publication Date

2018-03-01

DOI

10.1007/s00216-018-0924-y

Analytical and Bioanalytical Chemistry
https://doi.org/10.1007/s00216-018-0924-y

RESEARCH PAPER

Toward miniaturized analysis of chemical identity and purity of radiopharmaceuticals via microchip electrophoresis

Jimmy Ly[1,2,3] · Noel S. Ha[1,2] · Shilin Cheung[2,4] · R. Michael van Dam[1,2]

Received: 14 November 2017 / Revised: 19 January 2018 / Accepted: 29 January 2018

Abstract

Miniaturized synthesis of positron emission tomography (PET) tracers is poised to offer numerous advantages including reduced tracer production costs and increased availability of diverse tracers. While many steps of the tracer production process have been miniaturized, there has been relatively little development of microscale systems for the quality control (QC) testing process that is required by regulatory agencies to ensure purity, identity, and biological safety of the radiotracer before use in human subjects. Every batch must be tested, and in contrast with ordinary pharmaceuticals, the whole set of tests of radiopharmaceuticals must be completed within a short-period of time to minimize losses due to radioactive decay. By replacing conventional techniques with microscale analytical ones, it may be possible to significantly reduce instrument cost, conserve lab space, shorten analysis times, and streamline this aspect of PET tracer production. We focus in this work on miniaturizing the subset of QC tests for chemical identity and purity. These tests generally require high-resolution chromatographic separation prior to detection to enable the approach to be applied to many different tracers (and their impurities), and have not yet, to the best of our knowledge, been tackled in microfluidic systems. Toward this end, we previously explored the feasibility of using the technique of capillary electrophoresis (CE) as a replacement for the "gold standard" approach of using high-performance liquid chromatography (HPLC) since CE offers similar separating power, flexibility, and sensitivity, but can readily be implemented in a microchip format. Using a conventional CE system, we previously demonstrated the successful separation of non-radioactive version of a clinical PET tracer, 3′-deoxy-3′-fluorothymidine (FLT), from its known by-products, and the separation of the PET tracer 1-(2′-deoxy-2′-fluoro-β-D-arabinofuranosyl)-cytosine (D-FAC) from its α-isomer, with sensitivity nearly as good as HPLC. Building on this feasibility study, in this paper, we describe the first effort to miniaturize the chemical identity and purity tests by using microchip electrophoresis (MCE). The fully automated proof-of-concept system comprises a chip for sample injection, a separation capillary, and an optical detection chip. Using the same model compound (FLT and its known by-products), we demonstrate that samples can be injected, separated, and detected, and show the potential to match the performance of HPLC. Addition of a radiation detector in the future would enable analysis of radiochemical identity and purity in the same device. We envision that eventually this MCE method could be combined with other miniaturized QC tests into a compact integrated system for automated routine QC testing of radiopharmaceuticals in the future.

Jimmy Ly and Noel S. Ha contributed equally to this work.

Electronic supplementary material The online version of this article (https://doi.org/10.1007/s00216-018-0924-y) contains supplementary material, which is available to authorized users.

✉ R. Michael van Dam
mvandam@mednet.ucla.edu

[1] Department of Bioengineering, Henry Samueli School of Engineering and Applied Science, University of California Los Angeles, 420 Westwood Plaza, Los Angeles, CA 90095-7227, USA

[2] Crump Institute for Molecular Imaging and Department of Molecular and Medical Pharmacology, David Geffen School of Medicine, University of California Los Angeles, 650 Charles E Young Dr., Los Angeles, CA 90095-8352, USA

[3] Present address: Bioengineering and Therapeutic Sciences, UCSF, San Francisco, CA 94158, USA

[4] Present address: Trace-ability, Inc., 6160 Bristol Parkway Ste. 200, Culver City, CA 90230, USA

Published online: 22 February 2018

Keywords Capillary electrophoresis · Microchip electrophoresis · Positron emission tomography · Chemical purity analysis · Microfluidics · Quality control testing · Radiopharmaceuticals

Introduction

Microscale capillary electrophoresis (CE)-based devices are increasingly being used for high-resolution separations where portability, ease of integration, or small sample size are of particular importance. Recent examples include environmental analysis [1], biomolecular separations [2, 3], and mobile heath diagnostics [4].

Another field that can benefit from the advantages of such devices is nuclear medicine, particularly in assessing patient safety of freshly prepared batches of short-lived radiolabeled imaging tracers for positron emission tomography (PET) or single photon emission computed tomography (SPECT). PET and SPECT are real-time, 3D medical imaging techniques with exquisite specificity and sensitivity for visualizing particular biological/biochemical processes depending on the tracer used. The information from a PET or SPECT scan is used clinically in the diagnosis of many diseases, prediction of response to therapy, and monitoring response to therapy [5–8]. Imaging is also an indispensable research tool for uncovering mechanisms of disease initiation and progression, developing new therapies, and measuring and optimizing the pharmacokinetic properties of new therapeutic compounds [9]. In the case of PET, the majority of scans are currently performed using the glucose analog 2-[^{18}F]fluoro-2-deoxy-D-glucose ([^{18}F]FDG) since a wide range of conditions that can be detected via altered metabolism [10–12], but there is a growing interest in visualizing a wide range of biological processes and receptors using other tracers [13, 14].

Since PET tracers are classified as drug products by regulatory agencies, they must pass stringent quality control (QC) tests after their production for safety of the patient prior to injection. Unlike ordinary pharmaceuticals, the short lifetime of radiopharmaceuticals requires that they be produced in relatively small batches close to the geographical location where the patient is scanned. As described in regulatory documents (e.g., U.S. Pharmacopeia General Chapter <823> [15] and U.S. Food and Drug Administration 21 CFR Part 212 [16]) and several review articles [17, 18], each radiopharmaceutical batch must be evaluated for color and clarity, pH, radioactivity, radioisotope identity, chemical/radiochemical identity, radiochemical purity, residual solvents, chemical purity, pyrogenicity, and sterility. Performing and documenting the tests is cumbersome and time-consuming, and requires an array of expensive analytical chemistry equipment and significant dedicated lab space, and there is considerable interest in the development of automated and lower-cost approaches. Several efforts are underway to develop integrated QC testing instruments that automatically perform and document all of the required tests and calibrations, e.g., QC-1 [19] (Munster, Germany), Trace-ability [20] (Culver City, CA USA), and ABT Molecular Imaging Inc. [21, 22] (Louisville, TN USA). While potentially alleviating the labor burden, these systems are still based on conventional, macroscale instruments linked into an integrated system along with a sample distribution mechanism.

By replacing conventional analysis techniques with lab-on-a-chip technologies, it may be possible to achieve significant reductions in the size, cost, and complexity of automated QC testing platforms, and potentially to increase sensitivity [2, 23]. Commercial microscale devices already exist for testing of endotoxins [24], and there have been recent efforts to miniaturize some of the other tests, including radioactivity measurement [25], radioisotope identity (half-life) test [25], pH test [26], color and clarity test [26], and Kryptofix 2.2.2 test [27]. While these results represent an impressive step forward, high-resolution miniaturized chromatographic methods, suitable for assessment of chemical or radiochemical identity and purity across a wide range of tracers, are notably missing. Due to the potential presence of several impurities in each batch of PET tracer, and due to the wide variety of tracers and synthesis methods, performing these tests will likely require some kind of chromatographic separation followed by a radiation detector (e.g., gamma rays or positrons) and additional detectors for non-radioactive species (e.g., UV absorbance, refractive index, or pulsed amperometric detectors) to quantify each compound and ensure it is below permitted limits. The identity of each peak can be determined by matching the retention time to a reference standard (or by co-injection of the standard), or, in rare cases, via a mass detector.

In this paper, we focus on the development of a microscale CE-based device to replace the gold standard approach of high-performance liquid chromatography (HPLC) for this critical and challenging component of QC testing. We have been exploring CE methods due to the possibility of microchip implementation and corresponding reductions in size, cost, and complexity of the overall QC system. Microchip electrophoresis (MCE) has been shown capable of separating a vast range of analytes including large biomolecules (e.g., nucleic acids, proteins), peptides, and inorganic ions and chiral molecules [28, 29] simply by tuning the separation conditions. The versatility and separation power of CE have been noted to be equal to HPLC, or even better in some applications [30]. CE also avoids the use of high pressures, which simplifies the interface with other system components and eliminates the need for bulky and expensive high-pressure valves,

pumps, and fittings. Additional advantages of CE are the ability to miniaturize the QC system into a microfluidic chip measuring 25 mm × 75 mm or smaller that is operated via a compact electronic control system and power supply, and the extremely tiny sample consumption (typically nanoliters).

Conventional-scale CE separation of several ^{99m}Tc-labeled SPECT species from impurities has been reported [31], and we recently showed that two ^{18}F-labeled PET tracers, namely 3′-deoxy-3′-[^{18}F]fluorothymidine ([^{18}F]FLT) and 1-(2′-deoxy-2′-[^{18}F]fluoro-β-D-arabinofuranosyl) cytosine ([^{18}F]FAC), can be readily separated from impurities, including Kryptofix 2.2.2 (K222), using MEKC [32]. Compared to traditional HPLC/UV, we observed similar separation resolution and limits of detection (LOD), but reduction in analysis time in some cases, and several orders of magnitude reduction in buffer and sample consumption. (In typical HPLC analysis of radiopharmaceuticals, sample volume is on the order of 10–100 μL, the flow rate is 1–2 mL/min, and the analysis time may be 5–30 min, consuming 5–60 mL of mobile phase. On the other hand, in MCE, the buffer consumption can be as low as 100 μL and sample injection volume is typically in the nanoliter range or lower.) However, to the best of our knowledge, there have been no reports on the miniaturization of these approaches to analyze chemical species relevant to the testing of radiopharmaceuticals. Here we describe a proof-of-concept hybrid microfluidic CE device consisting of a hydrodynamic injection chip, a separation capillary, and a microfluidic optical absorbance detection chip to perform chemical identity and purity analysis of FLT and its known impurities. Potentially, with integration of a radiation detector in the future, this approach could also be used for radiochemical identity and purity tests. In addition, this approach could enable the fluid path to be inexpensive and disposable, reducing maintenance and eliminating the need for cleaning, further simplifying the testing process.

Materials and methods

Reagents

Sodium phosphate monobasic (NaH_2PO_4), sodium phosphate dibasic dihydrate (Na_2HPO_4), boric acid, sodium dodecyl sulfate (SDS), ammonium acetate, ethanol, sodium chloride (NaCl), sodium hydroxide (NaOH), thymine, thymidine, furfuryl alcohol (FA), 2′,3′-didehydro-3′-deoxythymidine (stavudine), and 3′ deoxy-3′-fluorothymidine (FLT) were purchased from Sigma–Aldrich (Milwaukee, WI, USA). Zidovudine impurity B (chlorothymidine, CLT) was purchased from LGC Standards (Wesel, Germany). Kryptofix2.2.2 (K222), 3-N-Boc-5′-Odimethoxytrityl-3′-O-nosyl-thymidine (Boc-FLT) were purchased from ABX (Radeberg, Germany).

All samples were prepared with 18 MΩ deionized water using a Milli-Q® Integral Water Purification system (EMD Millipore, Billerica, MA, USA). Phosphate buffer (PB; 30 mM) was prepared via titration 100 mM solutions of NaH_2PO_4 and Na_2HPO_4 and monitored with a pH meter (Mettler, Toledo, Easy five, Columbus, OH, USA). SDS (100 mM) in 30 mM phosphate buffer (SDS-PB) was prepared by dissolving SDS in 30 mM PB. All buffers were degassed prior to use.

Miniaturized CE system

We combined the three key components (injection, separation, and detection) into a hybrid MCE system (Fig. 1). One microfluidic chip, used for sample injection and containing the anode, was connected to the upstream side of a 60-cm-long, Teflon-coated fused silica capillary (75 μm I.D., 375 μm O.D; Polymicro, Phoenix, AZ, USA). A second microfluidic chip, used for sample detection and containing the cathode, was connected to the downstream side of the separation capillary. The capillary was connected to each chip via a port perpendicular to the channels within the chip.

All electronic components were connected to a digital acquisition (DAQ) module (USB 6211, National Instruments Corporation, Austin, TX, USA). A custom-written LabVIEW program (National Instruments Corporation, Austin, TX, USA) was used to coordinate the timing of all functions.

Injection chip

Though the commonly used technique of electrokinetic injection provides a very convenient means to inject samples in CE and MCE, this technique suffers from injection bias, i.e., solutes with higher electrophoretic mobilities are preferentially introduced, resulting in a difference between the composition of the original sample and that injected into the separation channel, as well as changing of the sample composition over time which interferes with repeat measurements [33, 34]. This bias and other sensitivities of this technique (to voltage, sample conductivity, sample pH, electrolysis, and the possibility of complex formation) [34] could prevent accurate assessment of diverse impurities in PET tracer samples. Thus, pressure-driven injection [34], which avoids the above injection bias, was used.

The design of the microfluidic injection chip, shown in Fig. 2A, was adapted from the report of Li et al. [35]. The chip was fabricated from poly(dimethylsiloxane) (PDMS) using multilayer soft lithography [36]. Fabrication details and connection to the upstream end of the capillary are included in the Electronic Supplementary Material (ESM). The chip enables a controlled amount of sample to be loaded from the sample inlet port into the separation channel by momentarily

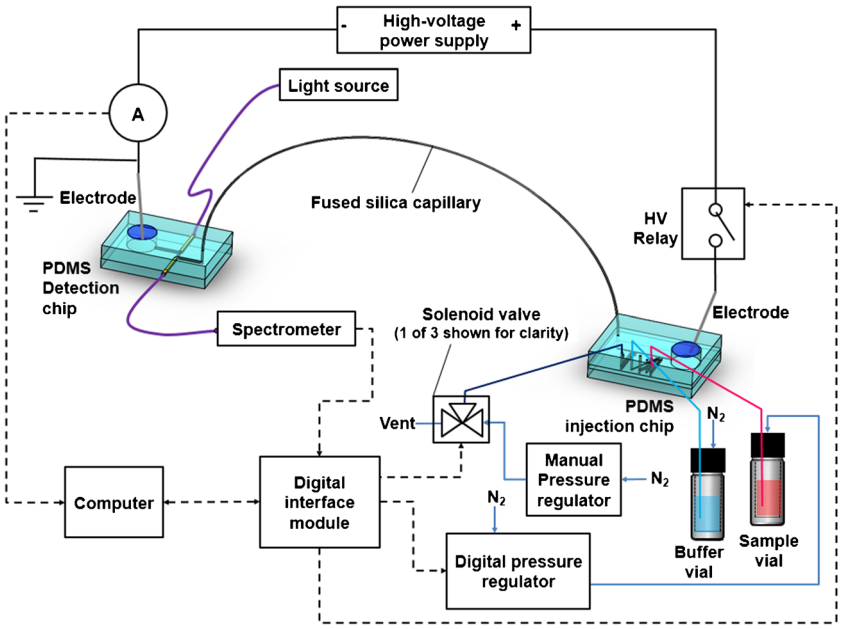

Fig. 1 Schematic of complete hybrid MCE device setup, including PDMS optical detection chip, PDMS injection chip, and glass capillary separation channel. The solenoid valves are used to control the on-chip microvalves

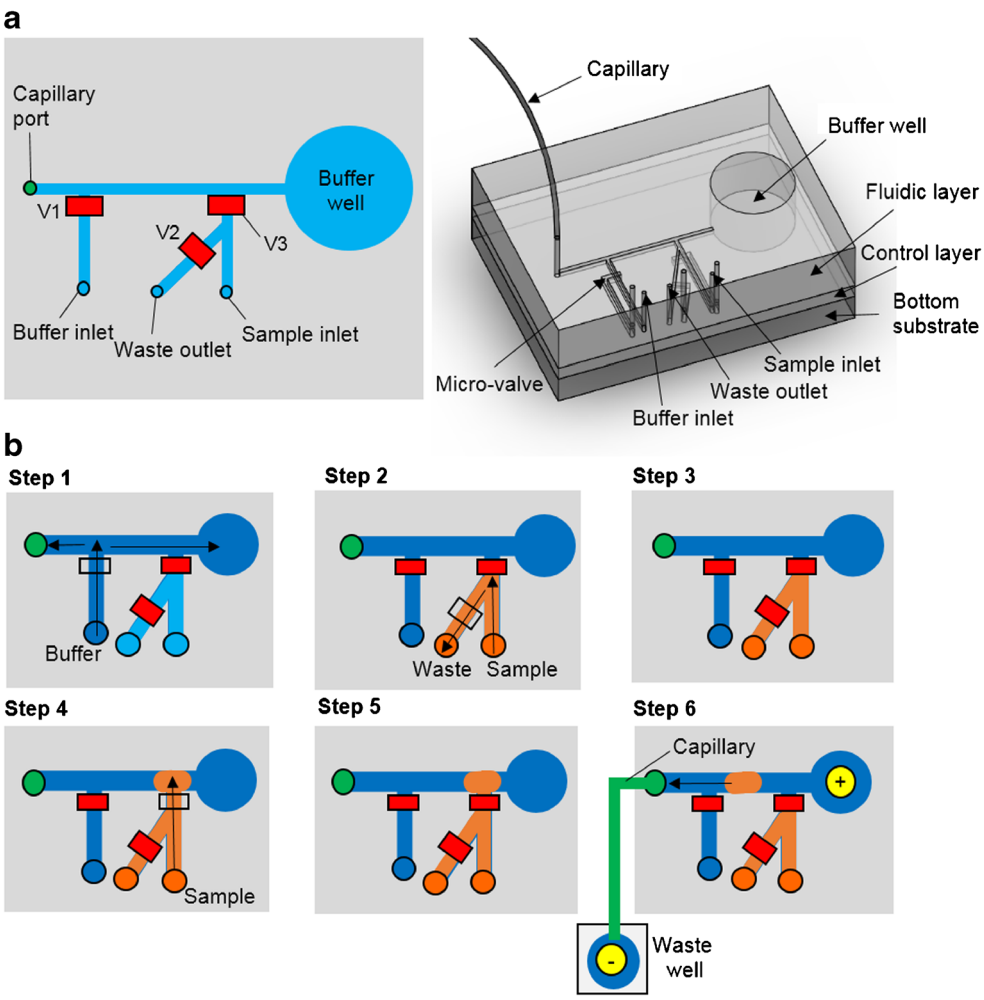

Fig. 2 **A** Design of multilayer PDMS chip for timed hydrodynamic sample injection. (left) Schematic; (right) 3D representation. **B** Schematic view of steps involved in injection process. First, the channel is primed with buffer (step 1). Next, the sample is loaded and primed (steps 2–3). The sample is then injected (steps 4–5), and the separation potential is applied along the separation channel (step 6). Solid red boxes indicate closed microvalves and hollow black boxes indicate open microvalves. Arrows indicate direction of fluid flow. Channels filled with buffer are shown in blue while those filled with sample are shown in orange. The capillary and waste well are connected for all steps but for clarity are only depicted in the final step when the separation voltage is applied. Diagrams not to scale

opening a microvalve (v3) for a fixed time. An additional microvalve (v2) enables priming of the sample inlet to eliminate air. The sample was contained in a septum-sealed vial (Fisherbrand™ 2 mL screw thread autosampler vial, Thermo Fisher Scientific, Waltham, MA, USA). Pressurized nitrogen gas was supplied to the vial through an electronic pressure regulator (ITV0010-3BL, SMC Corporation of America, Noblesville, IN, USA). The vial also contained an outlet tubing (#30 PTFE tubing, Cole-Parmer, IL, USA) connected to the sample inlet port of the injector chip. In addition to the sample inlet, the chip also contained an inlet for buffer solution, which was similarly connected to a pressurized vial of the separation buffer (SDS-PB) and controlled via microvalve v1.

The detailed steps to perform sample injection are illustrated in Fig. 2B. Before use, the chip was first primed with buffer by closing v3, opening v1, and pressurizing the buffer vial (6.0 psi) until buffer started flow out of all the buffer wells (and also out the buffer waste well of the detection chip connected to the other end of the capillary). Next, the sample vial was pressurized (1.5 psi) and the sample inlet was primed by closing v1 and v3 and then opening v2 until sample was seen entering the sample waste vial. To load the sample, valve v3 was then opened for a fixed time to allow sample to fill part of the main channel in the chip. After the sample is loaded, all valves were closed and electrophoretic potential was applied to separate the sample.

On-chip microvalves were each controlled by the common port of an electronic solenoid valve (S070B-5DG, SMC Corporation), connected to the chip via #30 PTFE tubing. The solenoid valves switched between two states: (i) supplying pressurized nitrogen (35 psi) to close the on-chip microvalve, and (ii) venting to atmosphere to allow the on-chip microvalve to open via elastic restoration of the PDMS. To avoid the generation of air bubbles inside the sample-containing channels of the chip, the valve control channels were filled with water prior to use as previously described [37].

Detection chip

In typical radio-HPLC systems used in the field of radiochemistry, the flow cell has a path length of ~ 10 mm (10,000 μm). In the case of capillary electrophoresis in capillaries or microchannels, the optical path length (OPL) is much shorter (e.g., 30–100 μm) if light is directed, via a window, perpendicular to the flow through the capillary of microchannel. Because this short optical path reduces the absorbance "signal," it typically results in a relatively poor LOD in CE systems compared to HPLC. This problem can be addressed by leveraging the ability to precisely control fluid geometry in microfluidic devices and implementing an increased optical path length. An in-plane Z-shaped detection cell design [38] was selected, due to the simplicity of chip fabrication and interfacing of the illumination and detection optical fibers.

The chip was fabricated from a single patterned layer of PDMS bonded to a PDMS substrate. Fabrication details, including connection to the downstream end of the capillary, are described in the ESM. The design (Fig. 3) includes fiber alignment channels to ensure accurate collinear alignment of both the optical fibers (i.e., to provide illumination via the external light source and detection via the external spectrometer) with a "jog" in the sample channel representing the extended optical path within the chip [39]. Due to the elastic property of PDMS, the 125-μm OD optical fibers (ThorLabs, Newton, NJ, USA) are held stably in these channels by friction forces. The flat ends of the fibers sit flush against the flat end of the fiber channels, providing efficient optical coupling to the sample channel. Since PDMS absorbs strongly in the UV range [40], it was desirable to minimize the thickness of PDMS membrane between the end of the fiber and the sample within the channel. A thickness of 100 μm was chosen as it provides good optical transmission (> 85% transmission for wavelengths > 220 nm), sufficient mechanical resistance to deformation, and high electrical breakdown voltage (~ 2000 V [41], sufficient to sustain the CE potential at this point in the separation channel). In addition to the portion of each fiber alignment channel that is collinear with the optical path, there is a continuation that allows the air initially in the channel to be vented. All channels were 125 μm deep and 125 μm wide. Using the same depth for the fiber-aligning channels as for the fluid-containing channels simplifies the chip fabrication, requiring a single thickness of photoresist.

The performance of the detection chip was compared with two combinations of light sources and detectors, one with lower performance and one with higher performance. Detector 1 comprised a PX-2 pulsed xenon light source (Ocean Optics, Dunedun, FL, USA) and USB-4000 spectrometer (Ocean Optics), and Detector 2 consisted of a DH-2000-BAL continuous deuterium light source (Ocean Optics) and QE-Pro spectrometer (Ocean Optics). The PX-2 is ~ 5× cheaper than the DH-2000-BAL; however, it has significant noise, which adversely affects LOD. The pulse-to-pulse variation in light intensity is in the range 3–12% depending on pulse frequency [42], compared to an intensity drift of < 0.01% per hour [43] for the DH-20000-BAL. Similarly, the USB4000 is ~ 20× cheaper than the QE-Pro, but has a lower signal-to-noise ratio (275:1 compared to 1000:1) and lower dynamic range.

While the current work serves as proof-of-concept for miniaturized analysis of PET radiopharmaceuticals, ultimately it will be necessary to incorporate a radiation detector with good spatial resolution to enable assessment of radiochemical identity and purity in addition to chemical purity. We are currently in the process of developing such an integrated detector for the detection chip and will publish these findings in the future.

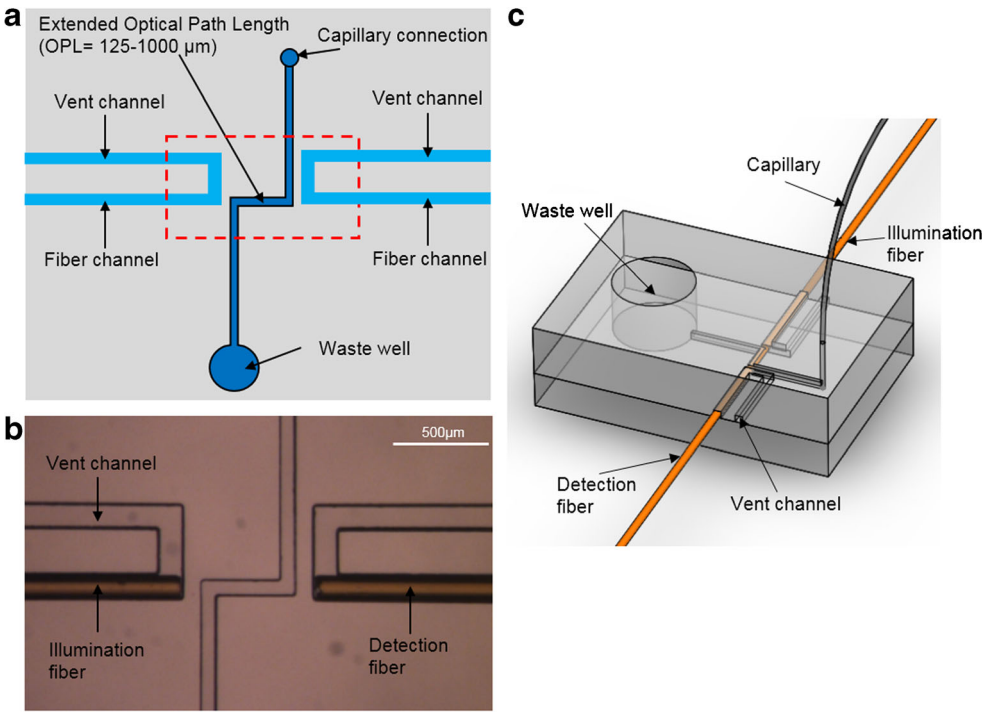

Fig. 3 **A** Schematic of the PDMS detection chip with the extended optical path. **B** Micrograph of the region of the chip outlined by the dotted red line in **A**. **C** 3D representation of the PDMS detection chip with connected capillary and optical fibers for absorbance measurement

Conditioning

After fabrication and assembly of the hybrid chip, it was conditioned prior to use. First, the chips and capillary were filled with water via the buffer inlet port at 10 psi for 30 min to ensure all air was purged from the system. The both ends of the chips were placed in a Petri dish containing a damp Kimwipe and wrapped with parafilm. Next, this procedure was repeated with 1 M NaOH to form hydroxyl groups [44] on the inner surfaces of the capillary and PDMS microchannels. The NaOH was removed during the buffer priming step of the sample injection process.

Separation

The separation voltage was provided by a 0–30-kV high-voltage DC power supply (HV350, Information Unlimited, Amherst, NH, USA). The tip of the high-voltage electrode wire was submerged in the separation buffer well of the injection chip and that of the ground electrode wire was submerged in the waste well of the detection chip. Electrodes were held in place by electrically insulated clamps mounted on a retort stand. Twelve kilovolts was supplied to achieve a field of ~ 200 V/cm along the separation channel. The total length of the separation path from the buffer well to the waste well was 62 cm. The effective separation length, i.e., injection point to the detector, was 61 cm. CE voltage was turned on or off using a solid-state relay in series with the high-voltage side of the circuit. During operation, DC current was monitored in real-time via a digital multimeter (Model 2831E, BK precision, Yorba Linda, CA, USA) to detect any abnormal behavior of the chip. For example, any air/gas bubble formation can lead to interruption of the current with intermittent electrical arcing; if this occurred, the high voltage was immediately interrupted and the fluidic system was reconditioned for ~ 2 min to purge any bubbles and to re-equilibrate the inner surfaces.

UV absorbance measurements

Methods for computing absorbance from the spectrometer signal are described in detail in the ESM. To create an electropherogram, spectrometer output was measured at a rate of 10 samples/s and converted to absorbance, starting at the time of injection.

Each electropherogram was analyzed using OriginPro 8.5 (OriginLab, Northampton, MA, USA) to determine peak migration times (t_m, taken at peak center), peak widths ($w_{1/2}$, full width at half maximum), as well as other values such as peak areas based on a Gaussian fit to each peak. Peaks were identified based on retention times determined by injecting standard compounds individually.

System characterization

Characterization of injection chip

For the purposes of characterizing the injector, the detection chip was not used; rather, detection of analytes was performed directly in the capillary using a four-way junction (PEEK

Cross, P-729, Idex Health & Science, Oak Harbor, WA, USA) positioned 7 cm away from the downstream end of capillary. A small portion of capillary was covered with a 1/16" OD tubing sleeve (Idex Health & Science, Oak Harbor, WA, USA) and secured via two opposite ports of the junction. The illumination and detection optical fibers were secured in the two perpendicular ports. Note that the effective separation length in this case was 54 cm. The total separation length between the buffer well of the injection chip and the waste vial was 61 cm and the separation voltage applied was + 12 kV.

To assess the sample injection repeatibility, successive injections of 5 mM thymidine were performed with a valve opening time of 800 ms (determined as described in the ESM).

Characterization of detection chip

Chemical purity tests are performed on radiopharmaceutical preparations to confirm the absence of impurities after the purification and formulation processes. For some impurities (e.g., Kryptofix K222, etc.), there are well-established limits based on toxicity studies that can safely be injected into patients. Unstudied impurities, provided they pose negligible risk of carcinogenicity, are typically limited to 1.5 μg per patient per day (5 nmol for a compound with molar mass of 300 g/mol). A typical radiopharmaceutical preparation has a volume of 1–10 mL (or larger) and contains sufficient material for one or more patient scans. In the conservative case (1 mL volume, 1 patient), this gives an upper permitted limit of 5 μM. To establish whether these levels can be detected in our setup, we have characterized the sensitivity of detection chip by measuring the LOD and limit of quantitation (LOQ) for varying conditions, including varying optical detection path length and varying optical systems.

To characterize the detection chip, the capillary was connected but the injection chip was not used. Instead, UV absorbance was measured when the detection chip was fully filled with several concentrations of each analyte. The absorbance was measured for each sample at the desired wavelength(s) for ~ 1 min, and then averaged to obtain one data point. This procedure was repeated three times while flushing the optical path length with blank solution between each measurement. The three data points were then averaged to obtain an overall absorbance value for the particular concentration of the particular analyte. To minimize the impact of cross-contamination, the most dilute samples were measured prior to more concentrated samples. After performing a linear fit of absorbance versus concentration (i.e., Beer's Law), the LOD and LOQ were determined by calculating the concentration that corresponds to 3× and 10×, respectively, the standard deviation in background absorbance noise. UV absorbance was measured at 256 or 224 nm, corresponding to the wavelength of maximum absorbance for the model compounds used (see ESM).

Evaluating separation efficiency

To evaluate separation efficiency, we chose as a model system the PET tracer [^{18}F]FLT, for which the impurity profile is well known [45]. The synthesis scheme and the structurally similar side-products are shown in Fig. 4. A mixture of FLT and by-products (5 mM thymidine, 2 mM thymine, 2.5 mM furfuryl alcohol, 5 mM stavudine, 2.6 mM FLT, and 1.4 mM CLT) was injected to assess separation efficiency. Separation was performed with micellar electrokinetic chromatography (MEKC) since the compounds are all neutral.

Samples were injected via injection chip using a valve opening time of 400 ms (determined as described in the ESM). For each peak in the resulting electropherogram, the number of theoretical plates, N, was calculated as follows [46, 47]:

$$N = 5.54\left(\frac{t_m}{w_{1/2}}\right)^2 \quad (1)$$

Benchmark comparisons

Performance was compared to separations on an analytical HPLC system as previously described [32]: Knauer Smartline HPLC system using a C18 Luna reverse phase column (4.6 mm × 250 mm, 5 μm; Phenomenex, Torrance, CA, USA). Detection was performed at 224 and 254 nm with an inline UV detector (model 2500, Knauer, Berlin, Germany). The HPLC mobile phase for FLT separations was 10% ethanol in water (*v*/*v*), at flow rate of 1 mL/min. All chromatograms were collected by a GinaStar analog to digital converter (Raytest USA Inc., Wilmington, NC, USA) and GinaStar software (Raytest USA Inc., Wilmington, NC, USA). Comparisons were also made to previously reported results using a commercial (macroscale) CE system (PA800, Beckman Coulter, CA, USA) [32].

Results and discussion

Sample injection

Injection repeatability of the PDMS injection chip was assessed by determining the consistency of peak area resulting from successive injections of single compound. The relative standard deviation (RSD) of peak area of successive injections of thymidine was 3.9% ($n = 8$). Since this performance was sufficient for remaining experiments to assess the feasibility of the hybrid MCE for chemical purity analysis, further

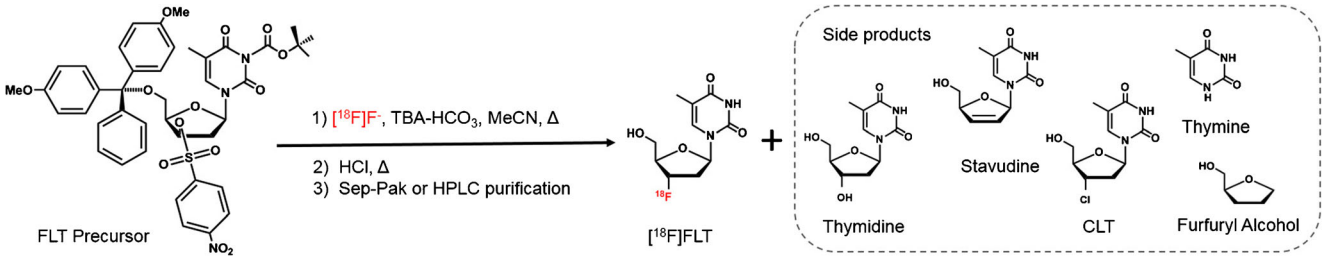

Fig. 4 Radiosynthesis of [^{18}F]FLT showing side-product formation. A mixture of FLT and side-products was used as a model system in this work. Figure adapted from [45], copyright © 2012, with permission of Elsevier

optimization was not performed at the time, and remaining results are performed with this injector.

However, peak area RSD < 2% is generally desired for quantitative analysis [48]. Li et al. reported a peak area RSD as low as 1.77% ($n = 15$) [35], using a similar PDMS injection chip, but with an integrated separation channel rather than external capillary as used here. We suspect that dead-volume at the chip to capillary junction in our MCE setup (see discussion below) may be causing the variability.

Another way to improve performance may be to switch injection methods since the method can have a large impact on the peak area RSD. In HPLC, the amount of sample is measured volumetrically (by the injection loop), resulting in very high injection repeatability. Recently, we explored a novel volumetric injection technique for MCE and showed that a peak area RSD as low as 1.04% ($n = 4$) [37] could be achieved, even using an external capillary for separation. We are thus confident that a next-generation device incorporating a PDMS-based injector will achieve sufficient repeatability for radiopharmaceutical analysis.

Sample detection

Initially, we attempted UV detection directly in the capillary. The LOD and LOQ for several analytes, using both combinations of light source and detector, are shown in Table 1. Even when the higher performance setup (Detector 2) was used for the in-capillary detection, LODs were all higher than 20 μM, and significantly worse than values previously measured for HPLC [32]. This is likely due to the much shorter optical path through the sample in the capillary, (i.e., ~75 μm, the inner diameter of the capillary) compared to the 10,000 μm flow cell in the HPLC system. The values were also significantly worse than those previously measured in a commercial CE system (5–11 μM; Beckman Coulter PA800) [32], likely due to differences in the optical system, capillary environment (i.e., temperature-controlled in the commercial CE system), and signal processing.

To improve the LOD, a PDMS detection chip with a Z-shaped extended optical path (500 μm) was implemented. In combination with the higher performance light source and detector pair (Detector 2), LODs ranged from 2 to 3 μM for the set of compounds with similar chromophore (thymidine, thymine, stavudine, FLT, and CLT), and 7 μM for furfuryl alcohol. Thus, the LOD values of the MCE setup are comparable to the performance of HPLC (i.e., 2 μM for stavudine and FLT, 35 μM for furfuryl alcohol) [32], and are below the typical permitted limit of impurities found in radiopharmaceuticals. Detection performance is summarized in Table 1 for all system configurations. Since the desired performance was achieved, the 500-μm OPL was used in subsequent experiments. For a 500-μm OPL detection chip and Detector Configuration 2, we found the linear range of the various species to be as follows: 2 μM–5 mM (thymidine), 2 μM–5 mM (thymine), 7 μM–3 mM (furfuryl alcohol), 3 μM–5 mM (stavudine), 3 μM–5 mM (CLT), and 2 μM–5 mM (FLT).

We also explored the possibility to achieve similar performance with the lower-performance (and lower cost) light source and detector (Detector 1) by fabricating additional detection chips with different OPL. The LOD and LOQ values for thymidine and furfuryl alcohol in detection chips with different OPL are summarized in Table 2. To more clearly see the effect of OPL, we note that LOD is defined as the concentration of analyte where the absorbance equals 3× the standard deviation of noise (N). Substituting into Beer's law, we can write $LOD = 3N/\varepsilon/OPL$, where ε is the molar absorbtivity. Thus, LOD is inversely proportional to the OPL and the data in Fig. 5 were thus fit to this function to extrapolate the OPL necessary to match the performance of HPLC. To achieve LOD = 2 μM for thymidine (and FLT and stavudine, which have an identical chromophore and thus similar absorbance), an OPL of 2500 μm would be required. Similarly, to achieve LOD = 35 μM for furfuryl alcohol, an OPL of 420 μm would be required. Thus, the PDMS detection chip with Detector 1 could match/surpass the detection sensitivity of HPLC by extending the optical path length to 2500 μm.

Separation of samples

Previously we showed that mixtures of FLT and its structurally similar by-products (thymidine, thymine, furfuryl alcohol, stavudine, and CLT) could be separated by HPLC and by a

Table 1 Limits of detection (LODs) and quantitation (LOQs) for all setups for FLT and its impurities. Blank entries indicate conditions that were not measured. By combining a higher performance light source and detector with 500 μm OPL (italic entries), the sensitivity of the MCE setup was comparable to HPLC (italic entries)

Experimental setup			Compound							
			Thymidine	Thymine	FA	Stavudine	FLT	CLT	K222	
MCE detection chip (with 500 μm OPL)	Detector 1 (lower performance)	Wavelength (nm)	256	256	224	256	256	256		
		LOD (μM)	8		30					
		LOQ (μM)	30		96					
	Detector 2 (higher performance)	LOD (μM)	*2*	*3*	*7*	*3*	*2*	*3*		
		LOQ (μM)	8	10	23	10	8	9		
In-capillary detection	Detector 1 (lower performance)	Wavelength (nm)	256	256	224	256	256	256		
		LOD (μM)	210	260	790	310	300	1100		
		LOQ (μM)	750	850	2600	1000	1000	3500		
	Detector 2 (higher performance)	LOD (μM)	22	21	54	27	25	75		
		LOQ (μM)	72	69	180	91	84	250		
HPLC		Wavelength (nm)			224	254	254		*	*
		LOD (μM)			*35*	*2*	*2*		Not detected	
		LOQ (μM)			116	4	5		Not detected	
Commercial CE		Wavelength (nm)	254	254	218	254	254	254	218	205
		LOD (μM)	5	5	11	7	6	6	180	120
		LOQ (μM)	13	14	36	15	20	15	570	390

*Measurements were attempted at various wavelengths (205, 218, 224, 236, 254, and 267 nm) but K222 could not be detected

conventional CE instrument with baseline resolution [32]. We analyzed similar samples to demonstrate the feasibility of injecting, separating, and detecting samples in the hybrid microfluidic system.

First, we started with the simplest geometry that resembles the commercial CE instrument, i.e., a capillary-only ("0-junction") system without any microchips connected (Fig. 6A). For this method, the injection was performed electrokinetically, by inserting the upstream side of the capillary in the sample vial (2 mL, C4013-15A, Thermo Scientific), applying + 12 kV for 5 s, then moving the capillary back to the buffer vial prior to separation. Successful baseline separation of the sample mixture (FLT and five impurities) was achieved (Fig. 7A).

Next, the injection microchip was added to the capillary to form a "1-junction" system (Fig. 6B). Even though baseline separation was observed for most peaks, the first two peaks were not completely resolved (Fig. 7B). Finally, we tested an integrated microfluidic system with injection chip, silica capillary, and detection chip (Fig. 6C). An electropherogram is shown in Fig. 7C. While all expected peaks are discernible, baseline separation was not achieved among the three fastest eluting compounds (thymidine, thymine, and furfuryl alcohol). Qualitatively, it is clear that the peak width using the hybrid MCE device was greater than that for the 0-junction setup, leading to the reduced separation efficiency. This was confirmed by computing the number of theoretical plates, N, for each setup (Table 3): it was found that N is significantly lower for the hybrid MCE device compared to the 0-junction setup.

To determine where improvements can be made, we analyzed another measure of efficiency: the plate height, $H = L/N$, where L is the effective separation length. Lower H values indicate more theoretical plates within the separation length, meaning a higher separation efficiency. Conveniently, H can be expressed as a sum of contributing factors (injection, detection, diffusion, and geometry) [49]:

$$H = \frac{L}{N} = H_{inj} + H_{det} + H_{diff} + H_{geo} \quad (2)$$

Table 2 Performance of PDMS detection chip with varying optical path lengths. Limit of detection (LOD) and quantitation (LOQ) are indicated for thymidine (256 nm) and furfuryl alcohol (224 nm). Measurements were performed with the lower performance light source and detector (Detector 1)

	Thymidine (256 nm)		Furfuryl alcohol (224 nm)	
OPL (μm)	LOD (μM)	LOQ (μM)	LOD (μM)	LOQ (μM)
125	40	130	130	430
250	18	56	56	190
375	11	36	36	120
500	8	30	30	96
1000	5	16	16	54

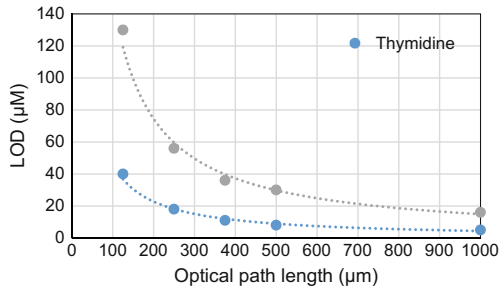

Fig. 5 Dependence of LOD on the OPL of the PDMS detection chip

The injection and detection components are determined from the length of the injection plug (l_{inj}) and the length of the detection cell (i.e., OPL) (l_{det}), respectively [49]:

$$H_{inj} = \frac{l_{inj}^2}{12L} \tag{3}$$

$$H_{det} = \frac{l_{det}^2}{12L} \tag{4}$$

where L is the effective separation length.

The contribution of axial diffusion [47, 49] is given by:

$$H_{diff} = \frac{2D_a}{\nu} \tag{5}$$

where D_a is the diffusion coefficient of the analyte and ν is the linear velocity of the analyte.

The contribution due to the geometry is the most complex [49, 50]:

$$H_{geo} = n\frac{(\omega\theta)^2}{12L} + \frac{\sigma_{ni}^2}{L} + \frac{\sigma_{dv}^2}{L} \tag{6}$$

The first term can be ignored since our system does not currently use a separation channel with a serpentine pattern (n is the number of turns, ω is the width at the top of the channel (peak of the turn), θ is the turn angle). σ_{ni} represents band broadening from non-ideal behavior of injected sample and Joule heating, and σ_{dv} represents the broadening due to dead-volume. Both σ_{ni} and σ_{dv} are of unknown form that depends of geometric shape of the channel, channel material, and electric field gradients [50].

Based on electropherograms, values of N, H, H_{inj}, and H_{det} were computed and are summarized in Table 3 (Detailed calculations can be found in the ESM). These results show that the contribution to peak broadening due to the detector (H_{det}) in the hybrid MCE (2-junction) device is negligible and broadening due to the injector (H_{inj}) is ~ 1% for stavudine and < 1% for CLT. Thus, the major contributors to the broadening of peak width are H_{diff} or H_{geo}.

For the 0-junction CE system, H (total) was low, i.e., 6.41 and 6.38 μm for thymidine and CLT, respectively. Based on the well-defined computed values of H_{inj} and H_{det}, and ignoring H_{geo} for the moment, maximum upper bounds on H_{diff} for the 0-junction system can be estimated as ~ 3.5 and ~ 5.2 μm for thymidine and CLT, respectively. It is expected that broadening due to diffusion (H_{diff}) would have a similar value for the 1- and 2-junction (hybrid MCE) systems. This is because the analytes, buffer, and temperature were

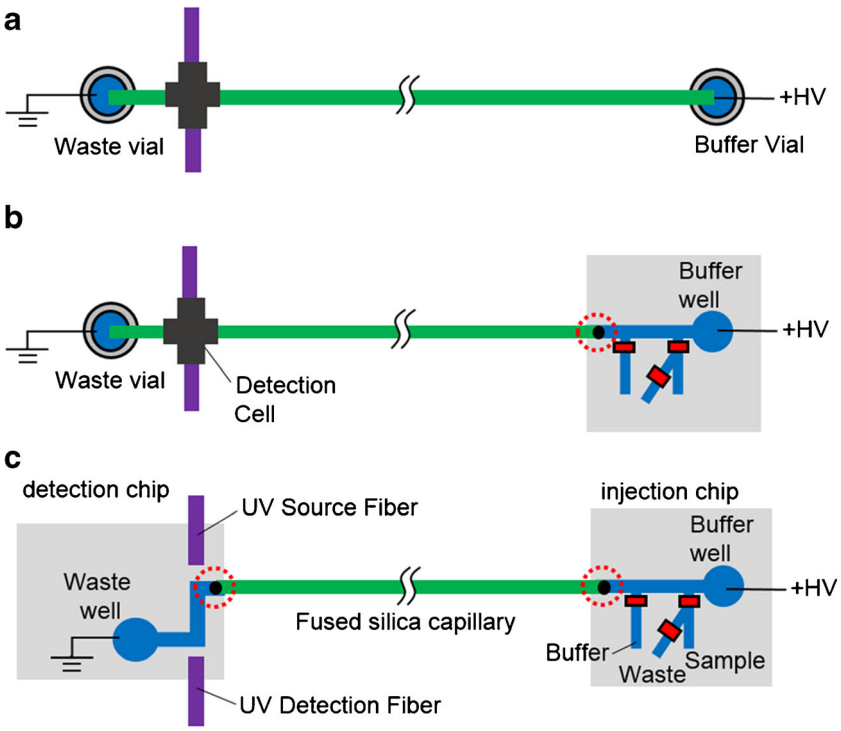

Fig. 6 Schematic of system configurations with different numbers of capillary-chip junctions. **A** Setup with the capillary-only (0-junction configuration). Sample was introduced via electrokinetic injection, and detection occurred in a capillary detection cell. **B** Setup with the PDMS injection chip and capillary (1-junction configuration). Detection occurred in a capillary detection cell. This setup was used for evaluation of the injection performance. **C** Hybrid MCE device with PDMS injection chip, capillary, and PDMS detection chip. Red dotted circles highlight capillary junctions. Diagrams not to scale

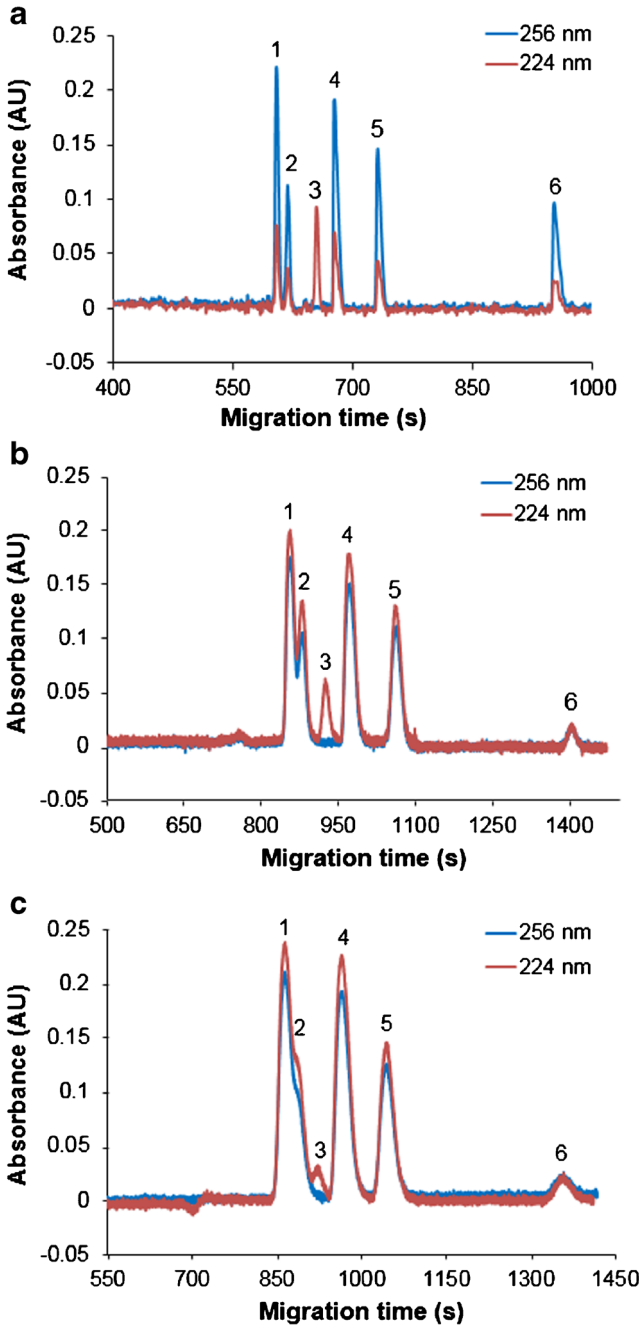

Fig. 7 Separation performance. **A** Electropherogram from separation in a capillary-only (0-junction) setup. Peaks: 6 mM thymidine (peak 1), 3 mM thymine (peak 2), 5 mM furfuryl alcohol (peak 3), 6 mM stavudine (peak 4), 3 mM FLT (peak 5), 3 mM CLT (peak 6). **B** Electropherogram from separation in a 1-junction setup (i.e., injection chip with a capillary). Peaks: 5 mM thymidine (peak 1), 2 mM thymine (peak 2), 2.5 mM furfuryl alcohol (peak 3), 5 mM stavudine (peak 4), 2.6 mM FLT (peak 5), and 1.4 mM CLT (peak 6). **C** Electropherogram of sample mixture injected, separated, and detected with the hybrid MCE device (i.e., with 2 capillary-chip junctions). Peaks: 5 mM thymidine (peak 1), 2 mM thymine (peak 2), 2.5 mM furfuryl alcohol (peak 3), 5 mM stavudine (peak 4), 2.6 mM FLT (peak 5), and 1.4 mM CLT (peak 6)

consistent across these systems and thus D_a was constant. In addition, the elution velocities were very similar (e.g., for CLT, 0-junction velocity was 0.054 cm/s, 1-junction velocity was 0.038 cm/s, and 2-junction velocity was 0.045 cm/s). Thus, we expect H_{diff} to have an upper bound of only a few μm for the 1- and 2-junction cases, and we can deduce that H_{geo} must be the dominant factor for both.

Comparing the CLT peak from the 0- and 1-junction cases, there was a large increase in H (i.e., from 6.4 to 39), and comparing the 1- and 2-junction cases, there was another large increase (i.e., from 39 to 121). Since there are only minor expected differences in the injection, detection, or diffusion components of plate height, these increases must be due to geometric factors. Because of the strong increase in H as the number of junctions increases, the band broadening is likely occurring due to the geometry (e.g., dead-volume) at each capillary-to-chip junction.

The dead-volume could be reduced by various approaches such as precise drilling [50] or molding the capillary port [51], or by tapering the capillary to fit directly in an in-plane microchannel [37, 52]. The geometry issue could also be addressed by integration of the separation channel directly into the chip (instead of using a capillary); this would eliminate the junctions altogether and simplify the overall setup, enabling a single integrated microfluidic device for injection, separation, and detection. Separation in PDMS channels has been reported by several groups [53, 54], though some have reported challenges in maintaining stable surface conditioning [55, 56]. An alternative may be to perform separation using an embedded capillary [57, 58]. With an optimized chip, one could expect the total plate height H to be similar to the 0-junction case. Indeed, the elimination of one junction shows significant improvement in separation (Fig. 6B), and elimination of both junctions shows further improvement (Fig. 6A), achieving baseline separation of FLT and five impurities. An optimized hybrid (2-junction) MCE system with improved capillary junction is therefore expected to be capable of similar baseline separation.

In addition to addressing the dead-volume at the capillary junctions in this manner, optimization of other parameters could also be explored to maximize separation efficiency. For example, applied electrical field can be increased to increase the velocity of analytes, which would reduce diffusive broadening, and either allow reduced separation times or enable the use of increased separation length.

Conclusions

The use of miniaturization to reduce the equipment size and shielding needed for the chemical purity analysis of PET tracers is expected to be a key part of streamlining the QC testing process, and ultimately the overall tracer production

Table 3 Separation performance for the CE setups with different numbers capillary-chip junctions. Migration time (t_m), peak full width at half maximum ($w_{1/2}$), number of theoretical plates (N), plate height (H), injection component of plate height (H_{inj}), and detection component of plate height (H_{det}) are shown for each. Values were calculated for the fastest and slowest eluting analytes, i.e., stavudine and CLT for 1- and 2-junction cases and for thymidine and CLT for the 0-junction case

Analytical method	MCE												
No. cap junction	0						1				2		
Compounds	Thymidine	Thymine	FA	Stavudine	FLT	CLT	FA	Stavudine	FLT	CLT	Stavudine	FLT	CLT
t_m (s)	610	630	670	690	750	980	920	970	1070	1400	970	1050	1360
W1/2 (s)	5	5	5	7	7	8	15	17	21	28	22	30	45
N	82,400	88,100	99,200	54,200	63,600	82,800	21,000	18,100	14,300	13,900	10,700	6780	5060
H (μm)	6.43	6.01	5.34	9.78	8.33	6.40	26	30	38	39	57	90	121
Hinj (μm)	2.96	2.78	2.47	2.30	1.96	1.15	0.65	0.58	0.48	0.28	0.67	0.42	0.25
Hdet (μm)	9.01E−04	9.01E−04	9.01E−04	9.01E−04	9.01E−04	9.01E−04	2.93E−03	2.93E−03	2.93E−03	2.93E−03	0.034	0.034	0.034
Number of repeats (n)	3	3	3	3	3	3	4	4	4	4	3	3	3

process. In this work, we have demonstrated the first proof-of-concept experiments to show the feasibility of microfluidic implementation of chemical identity and purity tests of radiopharmaceuticals.

The novel hybrid MCE device consists of a PDMS injection chip, a silica capillary, and a PDMS detection chip. Sample injection was based on hydrodynamic injection using microvalves to achieve satisfactory reproducibility while avoiding the known injection bias of conventional electrokinetic injection. The detection chip enabled adjustment of the optical path length to tune the limit of detection. Though an extended path length of 500 μm resulted in LOD comparable to HPLC when the higher performance light source/detector pair was used, we showed that further extension of the optical path (e.g., OPL ~2500 μm) could enable similar sensitivity even with the lower performance light source and detector, without significantly compromising the separation performance. In the integrated hybrid device, mixtures of FLT and impurities were successfully injected, separated, and detected. Even though FLT was successfully separated from all impurities, several impurity peaks were not fully resolved with baseline resolution. While the separation performance of the integrated device was lower than desired, a detailed analysis identified the capillary-chip junctions as the problem. Extrapolating from the performance when junctions are eliminated, we argue that a device with optimized junctions [37] could achieve the requisite performance. Furthermore, the optimized MCE device would be very much smaller than an HPLC system.

Unlike simple colorimetric tests that have been developed for determination of certain individual impurities (e.g., Kryptofix 2.2.2, a phase transfer catalyst frequently used in the synthesis of ^{18}F-labeled PET tracers), MCE-based testing provides a flexible way to assess different and multiple impurities, possibly by tuning separation conditions and/or adding detectors (e.g., electrochemical, pulsed amperometric, etc.) for detection of species with low UV absorbance. Furthermore, separation prior to detection greatly reduces the chance of false negatives or positives due to non-specific interactions that can occur in colorimetric tests. Due to the flexibility of a chromatographic approach, it is expected that this device could easily be applied to the evaluation of PET tracers other than FLT. Furthermore, integration of a radiation detector would enable assessment of radiochemical identity and purity in the same device.

In the long term, this device and other microfluidic QC tests could be combined in a unified lab-on-a-chip device for performing fully automated QC testing of radiopharmaceuticals. In addition to alleviating the burden of performing and documenting QC tests, such a system would reduce the amount of sample consumed for analysis, reduce the radiation exposure to personnel, and potentially reduce the time needed to complete all QC tests.

Funding This work was supported in part by the Department of Energy Office of Biological and Environmental Research (DE-SC0001249), the National Institute on Aging (R21AG049918), and the National Cancer Institute (U54 CA151819A, i.e., the Caltech/UCLA Nanosystems Biology Cancer Center).

Compliance with ethical standards

Conflict of interest The authors declare that they have no conflict of interest.

References

1. Ueland M, Blanes L, Taudte RV, Stuart BH, Cole N, Willis P, et al. Capillary-driven microfluidic paper-based analytical devices for lab on a chip screening of explosive residues in soil. J Chromatogr A. 2016;1436:28–33. https://doi.org/10.1016/j.chroma.2016.01.054.
2. Tetala KKR, Vijayalakshmi MA. A review on recent developments for biomolecule separation at analytical scale using microfluidic devices. Anal Chim Acta. 2016;906:7–21. https://doi.org/10.1016/j.aca.2015.11.037.
3. Fanali S. An overview to nano-scale analytical techniques: nano-liquid chromatography and capillary electrochromatography. Electrophoresis. 2017;38:1822–9. https://doi.org/10.1002/elps.201600573.
4. D'Ambrosio MV, Bakalar M, Bennuru S, Reber C, Skandarajah A, Nilsson L, et al. Point-of-care quantification of blood-borne filarial parasites with a mobile phone microscope. Sci Transl Med. 2015;7:286re4–4. https://doi.org/10.1126/scitranslmed.aaa3480.
5. Phelps ME. PET: the merging of biology and imaging into molecular imaging. J Nucl Med. 2000;41:661–81.
6. Bansal A, Pandey MK, Demirhan YE, Nesbitt JJ, Crespo-Diaz RJ, Terzic A, et al. Novel 89Zr cell labeling approach for PET-based cell trafficking studies. EJNMMI Res. 2015;5:19. https://doi.org/10.1186/s13550-015-0098-y.
7. Mariani G, Bruselli L, Kuwert T, Kim EE, Flotats A, Israel O, et al. A review on the clinical uses of SPECT/CT. Eur J Nucl Med Mol Imaging. 2010;37:1959–85. https://doi.org/10.1007/s00259-010-1390-8.
8. Bailey DL, Willowson KP. An evidence-based review of quantitative SPECT imaging and potential clinical applications. J Nucl Med. 2013;54:83–9. https://doi.org/10.2967/jnumed.112.111476.
9. Jackson IM, Scott PJH, Thompson S. Clinical applications of radiolabeled peptides for PET. Semin Nucl Med. https://doi.org/10.1053/j.semnuclmed.2017.05.007.
10. Banister S, Roeda D, Dolle F, Kassiou M. Fluorine-18 chemistry for PET: a concise introduction. Curr Radiopharm. 2010;3:68–80. https://doi.org/10.2174/1874471011003020068.
11. Weber WA, Figlin R. Monitoring cancer treatment with PET/CT: does it make a difference? J Nucl Med. 2007;48:36S–44.
12. Glaudemans AWJM, de Vries EFJ, Galli F, Dierckx RAJO, Slart RHJA, Signore A. The use of 18F-FDG-PET/CT for diagnosis and treatment monitoring of inflammatory and infectious diseases. Clin Dev Immunol. 2013;2013:1–14. https://doi.org/10.1155/2013/623036.
13. Marchand P, Bekaert V, Ouadi A, Laquerriere P, Brasse D, Curien H. Forty years of 18F-labeled compound development in an open access database. J Nucl Med. 2013;54:15N–7N.
14. Radiosynthesis Database of PET Probes (RaDaP). http://www.nirs.qst.go.jp/research/division/mic/db2/. Accessed 8 May 2017.
15. Radiopharmaceuticals for Position Emission Tomography – Compounding. Chapter 823. Radiopharmaceuticals for position emission tomography—compounding. U. S. Pharmacopeial Conv Natl Formul. 2009; 398–406.
16. CFR - Code of Federal Regulations Title 21. http://www.accessdata.fda.gov/scripts/cdrh/cfdocs/cfcfr/CFRSearch.cfm. Accessed 30 Jun 2013.
17. Fermi E. Quality control of PET radiopharmaceuticals. In: Molecular imaging: radiopharmaceuticals for PET and SPECT. Berlin: Springer; 2009. p. 197–204.
18. Scott PJH, Hockley BG. Radiochemical syntheses, radiopharmaceuticals for positron emission tomography. Hoboken: Wiley; 2011.
19. QC1 Automatic quality control for PET and MI tracers. In: http://www.qc1.com. http://www.qc1.com/. Accessed 20 Nov 2017.
20. Trace-ability, Inc.-SBIR Source. In: SBIRSource.com. http://sbirsource.com/sbir/firms/26162-trace-ability-inc. Accessed 26 Dec 2015.
21. Anzellotti AI, McFarland AR, Ferguson D, Olson KF. Towards the full automation of QC release tests for [18F]fluoride-labeled radiotracers. Curr Org Chem. 2013;17:2153–8.
22. Awasthi V, Watson J, Gali H, Matlock G, McFarland A, Bailey J, et al. A "dose on demand" biomarker generator for automated production of [18F]F- and [18F]FDG. Appl Radiat Isot. 2014;89:167–75. https://doi.org/10.1016/j.apradiso.2014.02.015.
23. Patabadige DE, Jia S, Sibbitts J, Sadeghi J, Sellens K, Culbertson CT. Micro total analysis systems: fundamental advances and applications. Anal Chem. 2016;88(1):320–38. https://doi.org/10.1021/acs.analchem.5b04310.
24. Charles River Laboratories, Inc. Endotoxin testing systems. http://www.criver.com/products-services/rapid-micro/endosafe/endotoxin-rapid-testing-systems. Accessed 16 Sep 2017.
25. Taggart MP, Tarn MD, Esfahani MMN, Schofield DM, Brown NJ, Archibald SJ, et al. Development of radiodetection systems towards miniaturised quality control of PET and SPECT radiopharmaceuticals. Lab Chip. 2016;16:1605–16. https://doi.org/10.1039/C6LC00099A.
26. Tarn MD, Isu A, Archibald SJ, Pamme N. On-chip absorbance spectroscopy for the determination of optical clarity and pH for the quality control testing of [^{18}F]FDG radiotracer. Proceedings of the 18th International Conference on Miniaturized Systems for Chemistry and Life Sciences. October 26–30, 2014, San Antonio. 2014;1077–79.
27. Charles OC. Radioanalysis for PET imaging pharmaceuticals: on-chip detection of Kryptofix 2.2.2. Int J Sci Eng Res. 2016;7:478–94.
28. Pagaduan JV, Sahore V, Woolley AT. Applications of microfluidics and microchip electrophoresis for potential clinical biomarker analysis. Anal Bioanal Chem. 2015;407:6911–22. https://doi.org/10.1007/s00216-015-8622-5.
29. Dawod M, Arvin NE, Kennedy RT. Recent advances in protein analysis by capillary and microchip electrophoresis. Analyst. 2017;142:1847–66. https://doi.org/10.1039/C7AN00198C.
30. Holzgrabe U, Brinz D, Kopec S, Weber C, Bitar Y. Why not using capillary electrophoresis in drug analysis? Electrophoresis. 2006;27:2283–92. https://doi.org/10.1002/elps.200600016.
31. Jankowsky R, Noll B, Johannsen B. Capillary electrophoresis of 99mtechnetium radiopharmaceuticals. J Chromatogr B Biomed Sci Appl. 1999;724:365–71. https://doi.org/10.1016/S0378-4347(98)00577-5.
32. Cheung S, Ly J, Lazari M, Sadeghi S, Keng PY, van Dam RM. The separation and detection of PET tracers via capillary electrophoresis for chemical identity and purity analysis. J Pharm Biomed Anal. 2014;94:12–8. https://doi.org/10.1016/j.jpba.2014.01.023.
33. Landers JP. Handbook of capillary electrophoresis, Second Edition. Boca Raton: CRC Press; 1996.
34. Saito RM, Coltro WKT, de Jesus DP. Instrumentation design for hydrodynamic sample injection in microchip electrophoresis: a

review. Electrophoresis. 2012;33:2614–23. https://doi.org/10.1002/elps.201200089.
35. Li MW, Huynh BH, Hulvey MK, Lunte SM, Martin RS. Design and characterization of poly(dimethylsiloxane)-based valves for interfacing continuous-flow sampling to microchip electrophoresis. Anal Chem. 2006;78:1042–51. https://doi.org/10.1021/ac051592c.
36. Studer V, Hang G, Pandolfi A, Ortiz M, Anderson WF, Quake SR. Scaling properties of a low-actuation pressure microfluidic valve. J Appl Phys. 2004;95:393–8. https://doi.org/10.1063/1.1629781.
37. Ha NS, Ly J, Jones J, Cheung S, van Dam RM. Novel volumetric method for highly repeatable injection in microchip electrophoresis. Anal Chim Acta. 2017;985:129–40. https://doi.org/10.1016/j.aca.2017.05.037.
38. Ro KW, Lim K, Shim BC, Hahn JH. Integrated light collimating system for extended optical-path-length absorbance detection in microchip-based capillary electrophoresis. Anal Chem. 2005;77:5160–6. https://doi.org/10.1021/ac050420c.
39. Liang Z, Chiem N, Ocvirk G, Tang T, Fluri K, Harrison DJ. Microfabrication of a planar absorbance and fluorescence cell for integrated capillary electrophoresis devices. Anal Chem. 1996;68:1040–6. https://doi.org/10.1021/ac950768f.
40. Ma B, Zhou X, Wang G, Dai Z, Qin J, Lin B. A hybrid microdevice with a thin PDMS membrane on the detection window for UV absorbance detection. Electrophoresis. 2007;28:2474–7. https://doi.org/10.1002/elps.200600619.
41. Technical Data Sheet: Momentive RTV615. Momentive Performance Materials Inc. Waterford, NY. https://www.momentive.com/en-us/products/tds/rtv615/.
42. Engineering Note: PX2 pulsed xenon lamp stability. Ocean Optics, Inc. Dunedin, FL, USA. 8 Jul 2002. https://oceanoptics.com/wp-content/uploads/PX2-Pulsed-Xenon-Lamp-Stability.pdf.
43. Ocean Optics DH-2000-BAL. In: Ocean Opt. http://oceanoptics.com/product/dh-2000-bal/. Accessed 28 Dec 2015.
44. Hoek I, Tho F, Arnold WM. Sodium hydroxide treatment of PDMS based microfluidic devices. Lab Chip. 2010;10:2283. https://doi.org/10.1039/c004769d.
45. Pascali C, Bogni A, Fugazza L, Cucchi C, Crispu O, Laera L, et al. Simple preparation and purification of ethanol-free solutions of 3′-deoxy-3′-[18F]fluorothymidine by means of disposable solid-phase extraction cartridges. Nucl Med Biol. 2012;39:540–50. https://doi.org/10.1016/j.nucmedbio.2011.10.005.
46. Jorgenson JW, Lukacs KD. Zone electrophoresis in open-tubular glass capillaries. Anal Chem. 1981;53:1298–1302. https://doi.org/10.1021/ac00231a037.
47. Giddings JC. Generation of variance, "theoretical plates," resolution, and peak capacity in electrophoresis and sedimentation. Sep Sci. 1969;4:181–9. https://doi.org/10.1080/01496396908052249.
48. Cianciulli C, Wätzig H. Analytical instrument qualification in capillary electrophoresis. Electrophoresis. 2012;33:1499–508. https://doi.org/10.1002/elps.201100699.
49. Jacobson SC, Hergenroder R, Koutny LB, Warmack RJ, Ramsey JM. Effects of injection schemes and column geometry on the performance of microchip electrophoresis devices. Anal Chem. 1994;66:1107–13. https://doi.org/10.1021/ac00079a028.
50. Bings NH, Wang C, Skinner CD, Colyer CL, Thibault P, Harrison DJ. Microfluidic devices connected to fused-silica capillaries with minimal dead volume. Anal Chem. 1999;71:3292–6.
51. Chiou C-H, Lee G-B. Minimal dead-volume connectors for microfluidics using PDMS casting techniques. J Micromech Microeng. 2004;14:1484.
52. DeLaMarre MF, Shippy SA. Development of a simplified microfluidic injector for analysis of droplet content via capillary electrophoresis. Anal Chem. 2014;86:10193–200. https://doi.org/10.1021/ac502272q.
53. Sahore V, Kumar S, Rogers CI, Jensen JK, Sonker M, Woolley AT. Pressure-actuated microfluidic devices for electrophoretic separation of pre-term birth biomarkers. Anal Bioanal Chem. 2015;408:599–607. https://doi.org/10.1007/s00216-015-9141-0.
54. Cong Y, Katipamula S, Geng T, Prost SA, Tang K, Kelly RT. Electrokinetic sample preconcentration and hydrodynamic sample injection for microchip electrophoresis using a pneumatic microvalve. Electrophoresis. 2016;37:455–62. https://doi.org/10.1002/elps.201500286.
55. Lacher NA, de Rooij NF, Verpoorte E, Lunte SM. Comparison of the performance characteristics of poly(dimethylsiloxane) and Pyrex microchip electrophoresis devices for peptide separations. J Chromatogr A. 2003;1004:225–35. https://doi.org/10.1016/S0021-9673(03)00722-2.
56. Vickers JA, Caulum MM, Henry CS. Generation of hydrophilic poly(dimethylsiloxane) for high-performance microchip electrophoresis. Anal Chem. 2006;78:7446–52. https://doi.org/10.1021/ac0609632.
57. Mecker LC, Martin RS. Integration of microdialysis sampling and microchip electrophoresis with electrochemical detection. Anal Chem. 2008;80:9257–64. https://doi.org/10.1021/ac801614r.
58. Sun X, Kelly RT, Danielson WF, Agrawal N, Tang K, Smith RD. Hydrodynamic injection with pneumatic valving for microchip electrophoresis with total analyte utilization. Electrophoresis. 2011;32:1610–8. https://doi.org/10.1002/elps.201000522.